S03120100-TRT10016
ORNL/TM-2024/3367

Neutronics Analysis of Heating and DPA of the Proton Beam Window and Core Vessel Nozzle of the Second Target Station

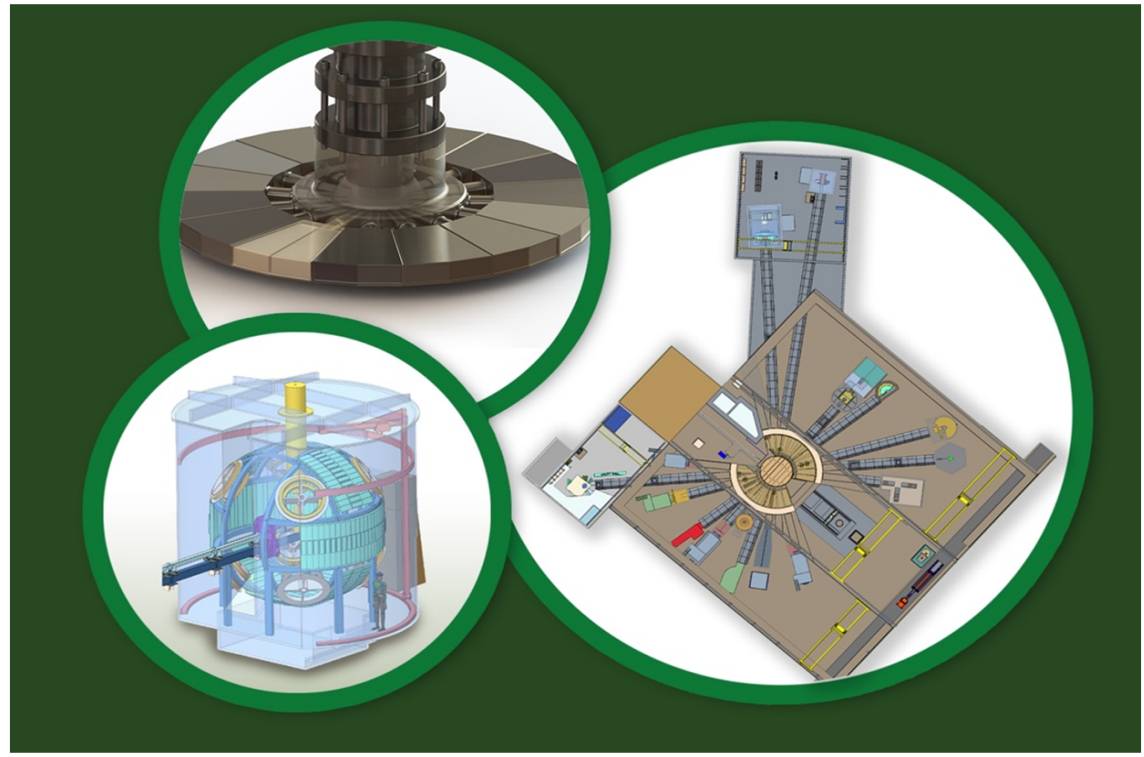

Kristel Ghoos

April 2024

Approved for public release.
Distribution is unlimited.

OAK RIDGE National Laboratory

ORNL IS MANAGED BY UT-BATTELLE LLC FOR THE US DEPARTMENT OF ENERGY

S03120100-TRT10016
ORNL/TM-2024/3367

Second Target Station Project

Neutronics Analysis of Heating and DPA of the Proton Beam Window and Core Vessel Nozzle of the Second Target Station

Kristel Ghoos

April 2024

Prepared by
OAK RIDGE NATIONAL LABORATORY
Oak Ridge, TN 37831
managed by
UT-Battelle LLC
for the
US DEPARTMENT OF ENERGY
under contract DE-AC05-00OR22725

Neutronics Analysis of Heating and DPA of the Proton Beam Window and Core Vessel Nozzle of the Second Target Station

Neutronics Analysis of Heating and DPA of the Proton Beam Window and Core Vessel Nozzle of the Second Target Station

LABORATORY ORNL	DIVISION/GROUP Second Target Station (STS) Project	CALC NO. S03120100-TRT10016
Prepared by Kristel Ghoos	Level III Manager Igor Remec	Lead Engineer Neelam Pradhan, Chris Anton

Other WBS elements affected
S031201, S0305, S0306

Signature/Date

	REV 0	REV 1	REV 2	REV 3
Prepared By				
Task Leader				
Level III Manager				
Checked By				
Lead Engineer				

CONTENTS

LIST OF FIGURES

LIST OF TABLES

ABBREVIATIONS

CSG	Constructive Solid Geometry
CV	Core Vessel
ORNL	Oak Ridge National Laboratory
PBW	Proton Beam Window
SNS	Spallation Neutron Source
STS	Second Target Station
UM	Unstructured Mesh

EXECUTIVE SUMMARY

This reports details the analysis of the heating rates, dpa values and He production in the Proton Beam Window (PBW) assembly and the Core Vessel (CV) nozzle for the preliminary design for the Second Target Station (STS). This analysis focuses on the heating rates in the cooled beltline component of the CV.

Neutronics calculations use a detailed unstructured mesh (UM) converted from a CAD model in SpaceClaim of the PBW and CV design of February 2024. The rest of the geometry is taken from the STS master model in constructive solid geometry (CSG). Heating is evaluated for four beam profiles, which are chosen as the most likely to produce the highest heating in the beltline component.

The maximum energy deposition values in the beltline are 0.02-0.08 J/cc/pulse, depending on the beam profile. Detailed point cloud data of the full UM geometry is made available for mechanical analysis. The maximum dpa rate in the beltline steel is approximately 0.02 dpa/year, which corresponds to a lifetime of 3,000 years. These results are in good agreement with previous results for the CV[1]. For the PBW itself, maximal heating, dpa, and He production rates are very similar to the previous analysis[2].

1 SCOPE

This analysis covers the heating, dpa and He-production rates in the Proton Beam Window (PBW) assembly and the Core Vessle (CV) nozzle of the February 2024 STS design. It focuses on the heating rates in the permanent, cooled shielding in the beltline from the CV to the PBW shielding. The analysis is performed for a beam profile with a 60 cm^2 and a 90 cm^2 footprint on the target. For both beam profiles, we evaluated the heating rates for the beam centered in the middle of the target and with a 6 mm horizontal and 4 mm vertical offset from the middle of the target. This displacement represents the largest nominal offset allowed for beam on operation. With an off-centered beam, the nozzle will locally be exposed to higher heating rates.

This analysis provides point cloud data of the energy deposition in the PBW assembly and CV nozzle to be used for further mechanical analysis for each beam profile. The dpa and He production rates, which are needed to evaluate the lifetime of the components, are only evaluated for the centered beam profile with a 60 cm^2 footprint.

This is in response to Neutronics Task Order 154, see https://ornl.sharepoint.com/:w:/r/sites/sts/targetsystems/_layouts/15/Doc.aspx?sourcedoc=%7B732401E1-EC36-4A41-A644-D6FAA0C15F0D%7D&file=TO-154_S.03.05_S.03.06_2024-02-14_PBW_shielding%20and%20CV%20nozzle%20to%20PBW-heating.docx&action=default&mobileredirect=true

2 ACCEPTANCE CRITERIA

Not applicable.

3 ASSUMPTIONS AND LIMITATIONS

Proton beam losses (1 W/m) are not included.

The mesh resolution in the beltline component is not sufficient to capture a smoothly resolved energy deposition profile in the inner part of the beltline component. As the largest values are not expected to cause problems, no further effort has been done to increase the resolution in this area. Further mechanical analysis needs to confirm if this assumption is valid.

4 METHODOLOGY AND MODELS

This MCNP geometry is a hybrid unstructured mesh (UM) / constructive solid geometry (CSG) model. The master model of the full STS facility is downloaded from the Devel branch on February 28, 2024. The CSG model includes a target, moderator reflector assembly, core vessel shielding, and monolith. The proton beam window (PBW) assembly and part of the core vessel (CV) geometry is modeled with UM using the SpaceClaim goemetry in `PBW_February_12_Reduced_SPACECLAIM_KG.scdoc`. The accelerator, downstream utilities, instrument halls, and high bay are not modeled. A vertical and horizontal cross-section view of the geometry is shown in Figures 1 and 2 respectively.

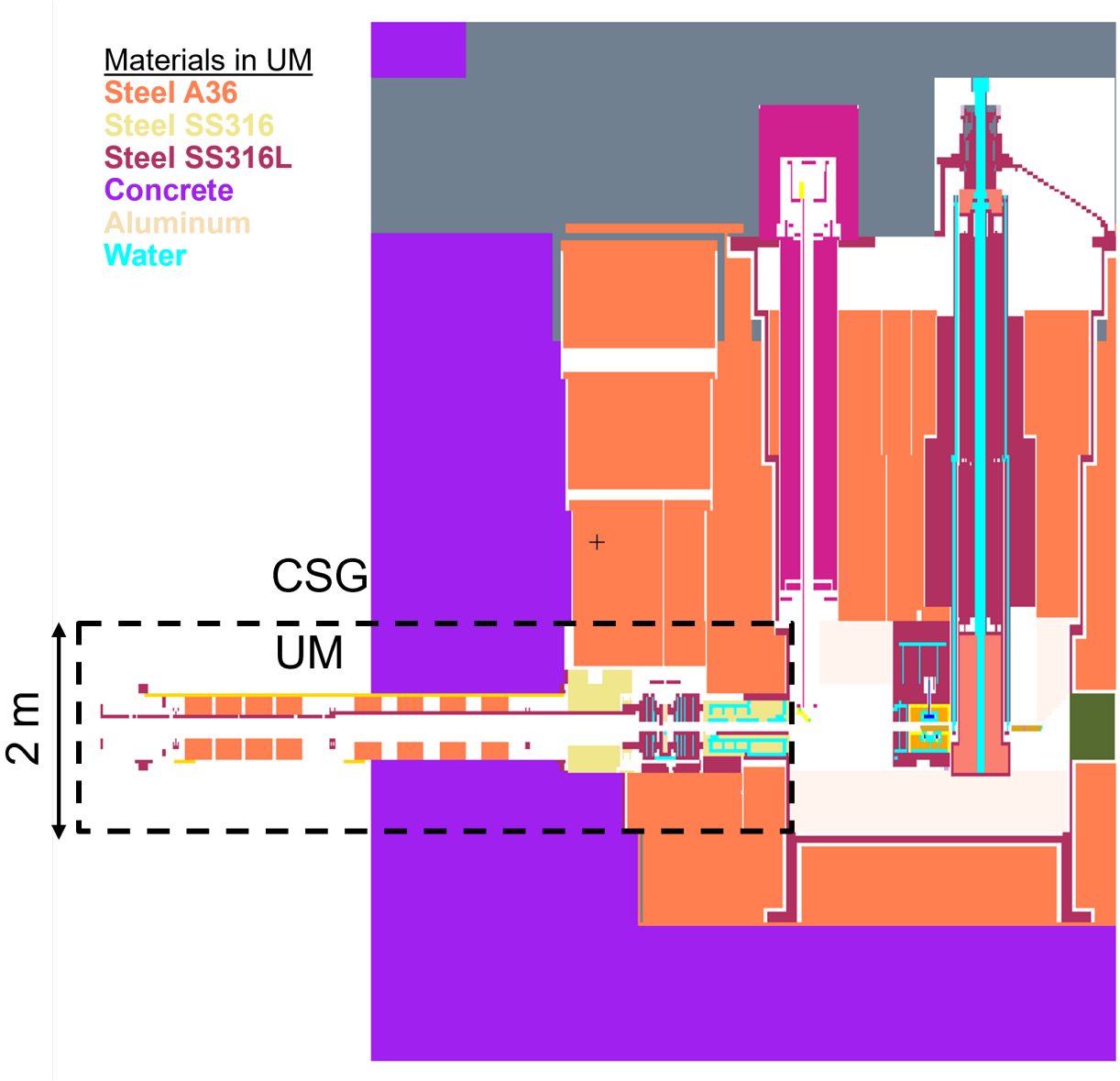

Figure 1. Vertical cross-section through the geometry with indication of the materials in the UM.

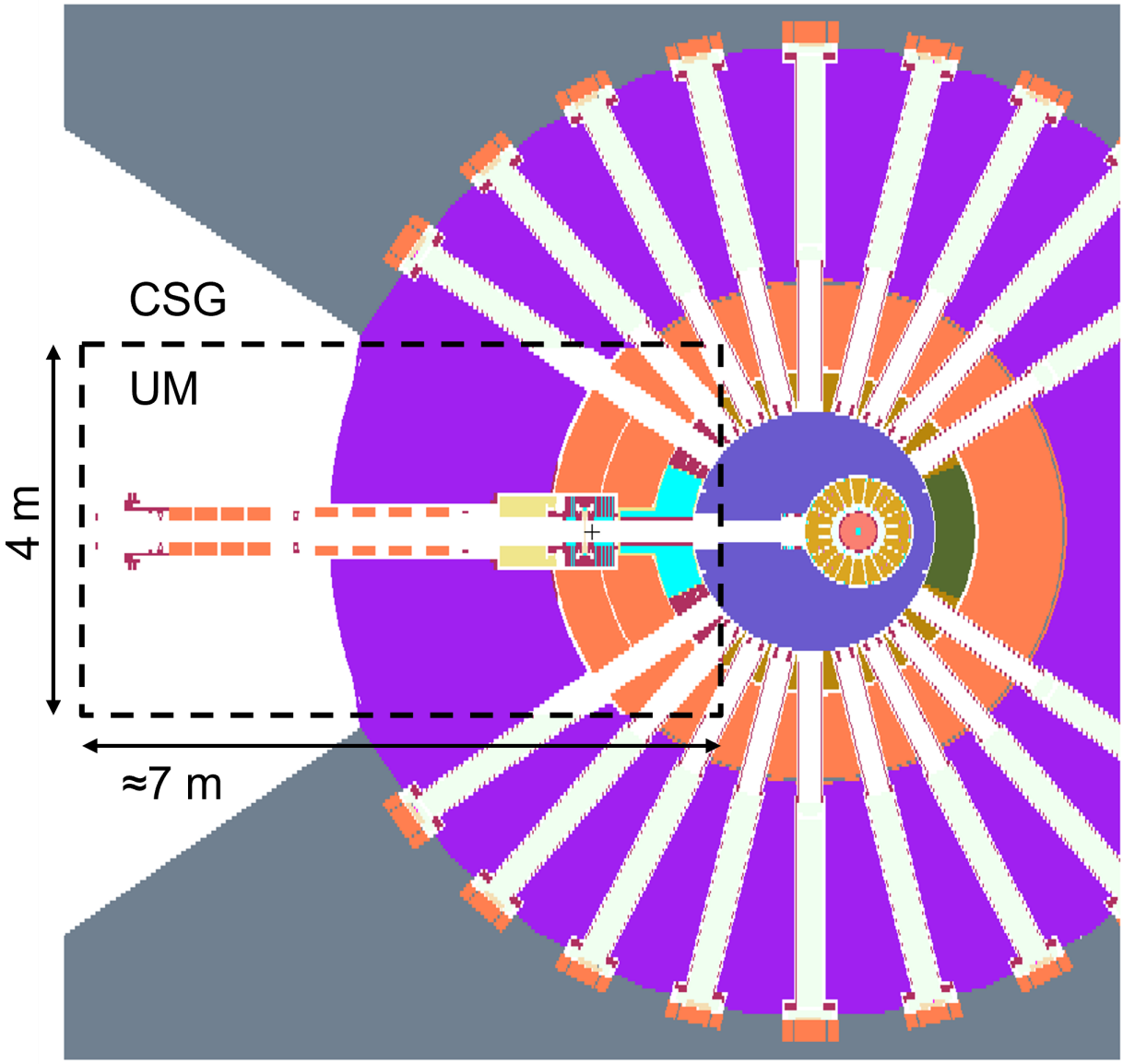

Figure 2. Horizontal cross-section through the geometry.

The UM is generated using Attila4MC [3]. The small, cylindrical water channels in the PBW have been approximated by hexagonal channels, which greatly simplifies the meshing process with very little loss of accuracy. To construct the unstructured mesh, the part-by-part mesh generator in Attila4MC is used. The full geometry is divided into six parts, based on the grouping used in the SpaceClaim model. While the undivided, full parasolid model did not succeed the mesh-generation process in Attila4MC, the individual parts were meshed without errors. No geometry errors were encountered when running the joined mesh in

MCNP. The mesh resolution in the PBW is chosen similar as in previous PBW analysis [2]: the components with the highest resolution (inner part of the PBW) have a maximum edge length of 2 cm and a minimum edge length of 1 cm in curvature refinement. The beltline and its water have mesh elements with a 4 to 6 cm maximum edge length and a minimum edge length of 1 cm for curvature refinement.

Beam profiles are chosen based on the highest expected heating in the nozzle of the CV beltline. The beam profiles are picked from a collection of realistic beam profiles, obtained from the Accelerator Systems group, post-processed for use in MCNP by Wouter de Wet. Looking at the height and width of the proton beam between about 1 m and 2 m upstream of the target face, the 60 cm^2 beam is the most extreme case for the vertical direction and the 90 cm^2 beam is the most extreme case for the horizontal direction. For both beams, the energy deposition is calculated with the beam centered exactly at the target center and with the beam centered about the maximum allowable offsets (4 mm vertically, 6 mm horizontally).

The dpa and He production analysis is performed with MCNP6.2[4], while the energy deposition analysis is performed with MCNP6.3[5]. This change was initiated by the substantial gain in computational time using MCNP6.3. For the same number of particles, MCNP6.3 runs more than twice as fast. To obtain sufficient statistics in the beltline component, approximately 10^8 particles were run for the energy deposition analyses. This takes approximately 2.5 days on 8 nodes (96 threads per node) on the STS-cluster Saturn per simulation. It is noteworthy to mention that the simulation had to be restarted with a different seed in the random number generator several times per analysis. No variance reduction was used.

The following partcles are tracked: neutrons, protons, photons, negative and positive muons, positive and negative pions, negative kaons, deuterons, tritons, helions, alphas. Neutral pions and short and long kaons are not tracked because of incompatibility errors in MCNP associated with the unstructured mesh. This is not expected to change the results significantly. In MCNP, this corresponds to mode card `mode n p | h ! / k d t s a * ?`. The particle types `z % ^` are not considered.

The post-processing is similar as in the 2022 PBW analysis described in [2]). The energy deposition in the mesh is calculated as the sum of the contributions of the protons, neutrons, photons, deuterons, tritons, alpha particles, and positive pions. To calculate the dpa, the neutron and proton fluxes are scaled by flux-to-dpa conversion factors. For the visualization of the results, we have used Paraview 5.12.0-RC3. The MCNP UM tally results have been converted to HDF5 format using a Python script [6].

5 ANALYSIS AND RESULTS

5.1 ENERGY DEPOSITION

Figure 3 shows the energy deposition in a vertical slice through the aluminum PBW for the four beam profiles. The white channels in this figure represent the location of the water channels. There is a clear difference in shape between the qd60 and qd90 profiles with respectively a 60 cm^2 and a 90 cm^2 footprint. This footprint refers to the surface area which encompasses 95% of the protons at the target face. As the protons do not travel purely in the X-direction but have a small divergence, the proton beam shape at the PBW, located approximately 250 cm before the target, is different than at the target face. For these beam profiles, the maximal energy deposition in the PBW reaches a higher value for the qd90 beam (5.8 J/cc/pulse) than with the qd60 beam (5.4 J/cc/pulse). The beam profiles with a maximal offset are translated from the nominal position by 4 mm vertically and 6 mm horizontally. This has a minimal effect on the energy deposition in the PBW.

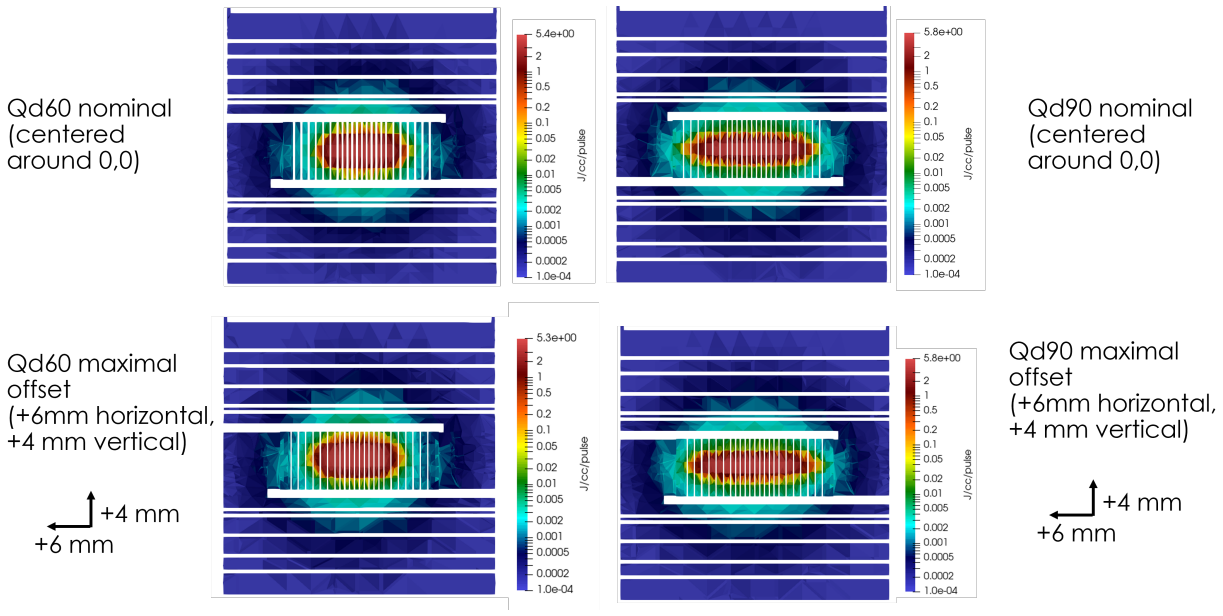

Figure 3. Vertical cross-section of energy deposition profile through PBW for four beam profiles. The water channels are shown in white.

Figures 4 and 5 show a vertical and horizontal slice through the energy deposition profile in the PBW and CV nozzle area for the four beam profiles. Table 1 lists the maximal values for the energy deposition in the PBW and beltline and the total energy deposition in the beltline for each beam profile. For both qd90 beam profiles, the maximum value is present in just one mesh element, with the heating value significantly lower (>10%) in the neighbouring elements. This indicates that the mesh resolution is too coarse to capture the gradients of the heating profile accurately. If this high value causes a concern, the simulation needs to be repeated with increased resolution. In general the energy deposition distribution looks very similar for all beam profiles. Also the total energy deposition in the beltline component changes very little with the beam.

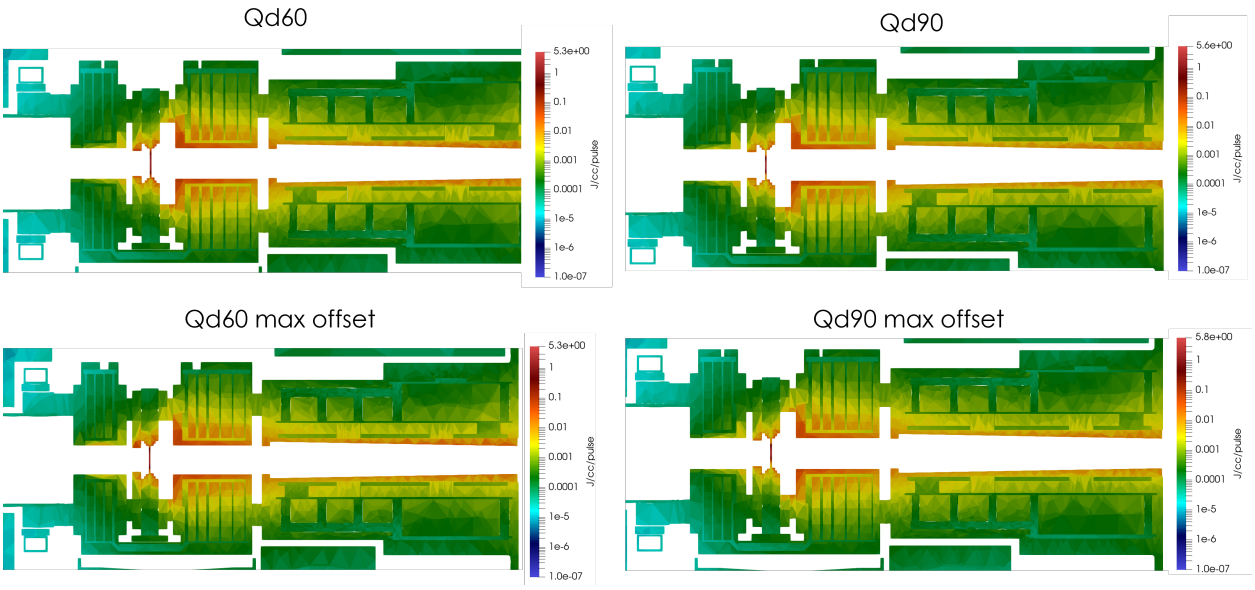

Figure 4. Energy deposition in a vertical cut through the geometry for the four beam profiles.

Table 1. Comparison of the maximal energy deposition value in the PBW and beltline and the total energy deposition in the beltline for the four beam profiles. The total volume in the beltline is 3.88E5 cm^3.

beam profile	max energy deposition in PBW (J/cc/pulse)	max energy deposition in beltline (J/cc/pulse)	total energy deposition in beltline (J/pulse)
qd60	5.4	0.02	169.5
qd60 maximal offset	5.4	0.03	172.7
qd90	5.8	0.05	175.5
qd90 maximal offset	5.8	0.08	177.0

Detailed point cloud data for the energy deposition of each beam profile is available in the sts-archive on saturn (see Appendix B). Further mechanical analysis will indicate whether further analysis is needed. More figures of the energy deposition in the full UM geometry, the beltline, and the cooling channels, including the statistical errors are given in Appendix C.

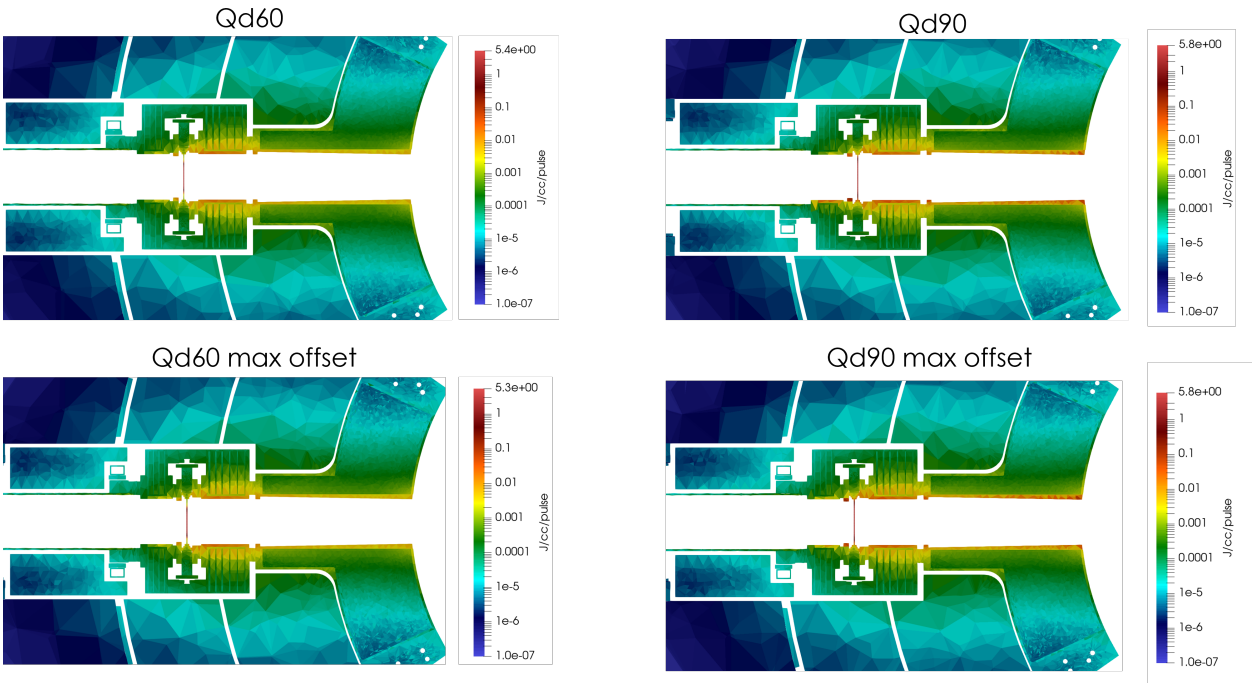

Figure 5. Energy deposition in a horizontal cut through the geometry for the four beam profiles.

5.2 DPA AND HELIUM PRODUCTION RATES

This section discusses the results for the dpa rates (in steel and aluminum) and helium production rates (in aluminum) for the qd60 beam profile. Figure 6 shows a vertical cut through the geometry of the map of the dpa rate in the steel components. The maximum value is 7.4e-11 dpa/pulse, which corresponds to 2.0e-2 dpa/year, assuming 5000 hours of operation per year at 15 Hz and 700 kW. This value is similar to the value of 1.2e-2 obtained in [2] and does not cause concern for the lifetime of the component. The maximum value in the beltline is 6.1e-11 dpa/pulse or 1.65e-2 dpa/year. With this rate, it takes 3,600 years to accumulate 60 dpa (lifetime limit). As this margin is very large, it inot necessary to repeat the calculation for the other beam profiles. These values are similar to the values previously obtained in [1] (maximum of 2.51e-11 dpa/pulse in the beltline).

Figure 7 shows the dpa rate (left) and He production rate (right) in a vertical cut through the aluminum PBW. The maximum values are again very similar to the values obtained in the 2022 analysis [2]. With a Helium production rate of 680 appm per year, the lifetime of the PBW is limited to 2.94 years, assuming a 2000 appm lifetime limit for aluminum. For the qd90 beam profile, the maximum Helium production rate is 740 appm per year, which corresponds to a lifetime of 2.70 years.

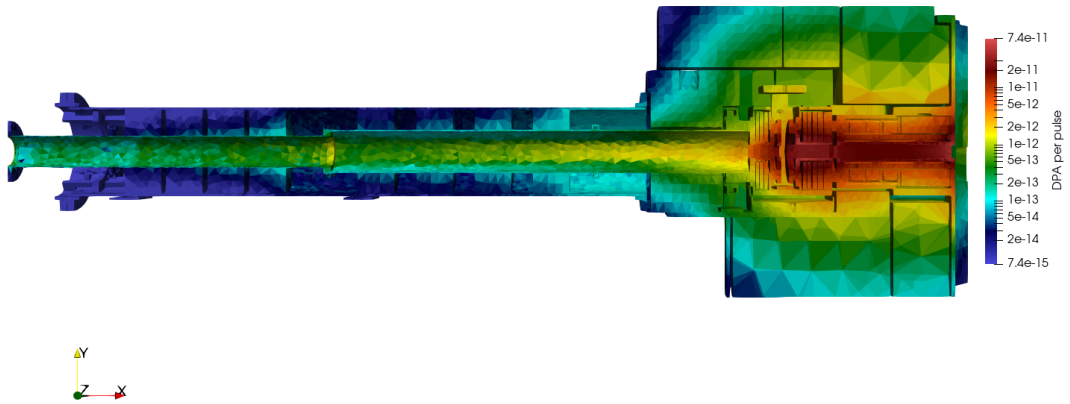

Figure 6. Dpa in a vertical cut through the steel components of the geometry for the qd60 beam profile.

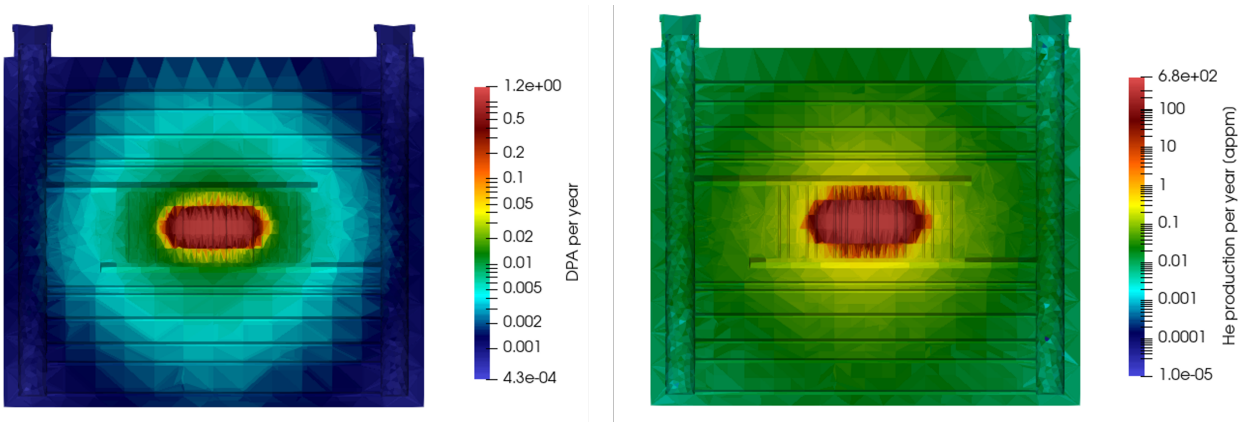

Figure 7. Dpa and He production in a vertical cut through aluminum PBW for the qd60 beam profile.

6 CONCLUSIONS

We performed a heating and dpa analysis for the proton beam window assembly and core vessel nozzle. We evaluated the energy deposition for four beam profiles, which correspond to the worst-case conditions in the beltline component in nominal operation. The highest heating rates in the beltline reach 0.02-0.08 J/cc/pulse depending on the beam profile and centering. Detailed point cloud data of the energy deposition is available for further mechanical analysis on saturn. The dpa rate in the beltline steel has a maximum value of approximately 0.02 per year and is not expected to be of concern for the facility's lifetime. In general, the results showed excellent agreement with previous results for the PBW assembly ([2]) and the core vessel ([1]).

7 ACKNOWLEDGEMENTS

The author would like to thank Hogan Knott, Wouter de Wet, and Lukas Zavorka for the support with this work.

8 REFERENCES

[1] L. Zavorka, "Neutronics heating and dpa analysis in the core vessel ." sts_archive/0-Task-Orders/TO-006_S.03.06_2022-01-26_CORE_VESSEL_HEATING on saturn, 2022.

[2] K. Ghoos, "Heating, dpa, and he production in the proton beam window assembly for the second target station," Tech. Rep. S03120100-TRT10008, ORNL/TM-2023/2912, Oak Ridge National Laboratory, 2023.

[3] *Attila4MC 10.2 Overview of Core Functions, Silver Fir Software, Inc., Gig Harbor, WA, USA, SFSW-UR-2020-OCF102*. 2020.

[4] C. Werner *et al.*, *MCNP User's Manual, Code Version 6.2, Los Alamos National Laboratory, LA-UR-17-29981*. 2017.

[5] J. A. Kulesza *et al.*, *MCNP Code Version 6.3 Theory and User Manual, Los Alamos National Laboratory, LA-UR-22-30006*. 2022.

[6] J. A. Kulesza and T. C. McClanahan, "A python script to convert mcnp unstructured mesh elemental edit output files to xml-based vtk files," Tech. Rep. LA-UR-19-20291, Los Alamos National Laboratory, 2018.

APPENDIX A. COMPUTER HARDWARE AND SOFTWARE

APPENDIX A. COMPUTER HARDWARE AND SOFTWARE

Calculations have been run on Saturn with the following modules:

- `attila/10.2.1`
- `mcnp/mcnp6.2mod_20231115`: for dpa and He production rate calculations
- `mcnp/mcnp6.3.0`: for energy deposition calculations.

On Windows, ParaView 5.12.0-RC3 has been used for visualization.

APPENDIX B. LOCATION OF COMPUTATIONAL INPUT AND OUTPUT FILES

APPENDIX B. LOCATION OF COMPUTATIONAL INPUT AND OUTPUT FILES

The input and output files are archived in the sts-archive on Saturn:
`sts_archive/0-Task-Orders/TO-154_S.03.05-S.03.06_2024-02-05_PBW_SHIELDING_AND_CV_NOZZLE`

APPENDIX C. FIGURES ON ENERGY DEPOSITION WITH CENTERED BEAM PROFILE QD60

APPENDIX C. FIGURES ON ENERGY DEPOSITION WITH CENTERED BEAM PROFILE QD60

Figure 8 and 10 gives more details on the energy deposition in the full UM geometry in respectively a vertical and horizontal slice through the geometry. The relative errors corresponding to these profiles are shown in Figures 9 and 11. In the corners of the geometry where the energy deposition is very low, the statistical error is above 20% (colored fully red). The regions with higher heating values are well converged with errors below 10% (colored in blue). Similar statistical precision is obtained for the heating values with the three other beam profiles.

Several 3D views of the cooled beltline component and the water in the UM model are given in Figures 12, 14, 16, and 18 with the relative errors in Figures 13, 15, 17, and 19.

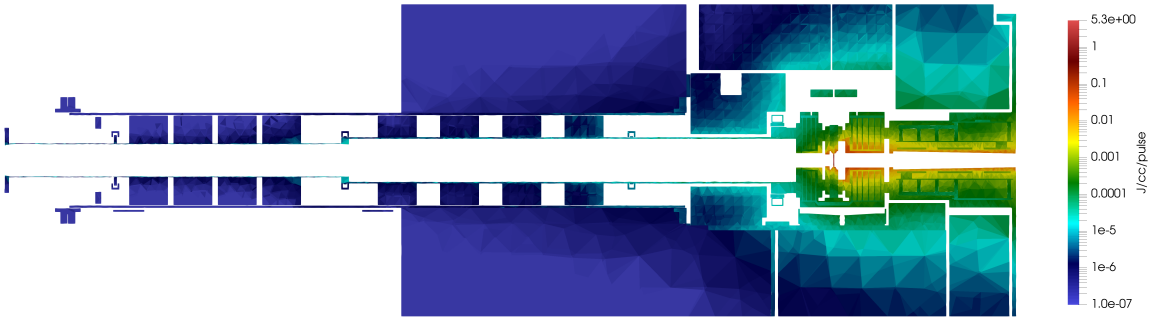

Figure 8. Energy deposition in a vertical cut through the geometry for the qd60 beam profile.

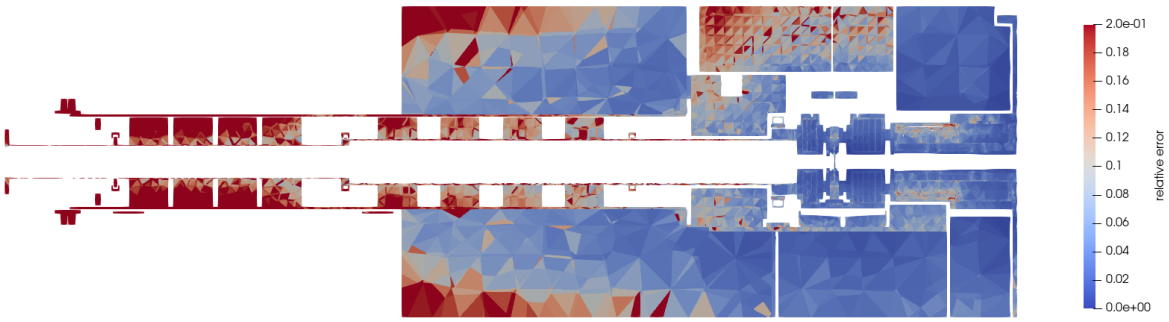

Figure 9. Statistical precision of the energy deposition data in a vertical cut through the geometry for the centered qd60 beam profile.

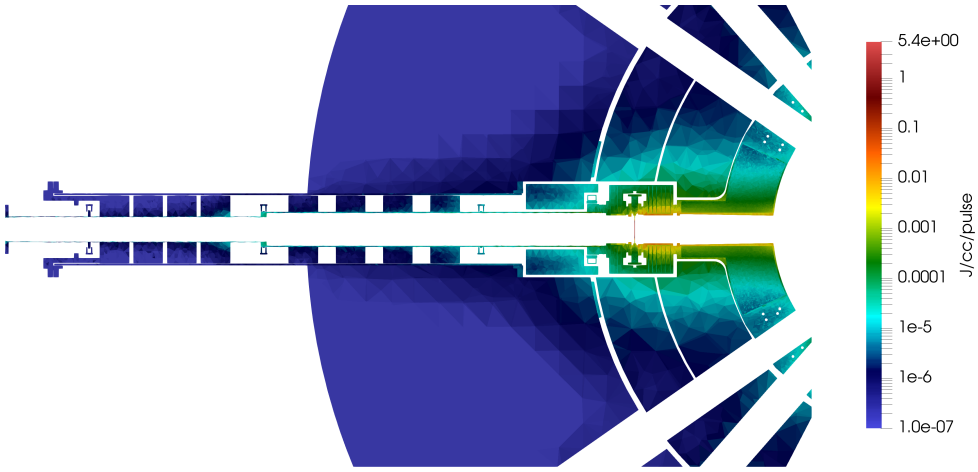

Figure 10. Energy deposition in a horizontal cut through the geometry for the centered qd60 beam profile.

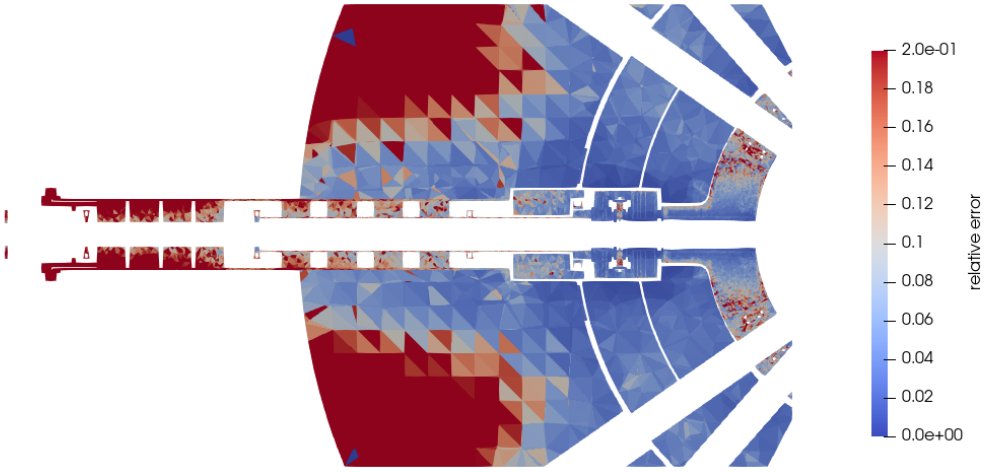

Figure 11. Statistical precision of the energy deposition data in a horizontal cut through the geometry for the centered qd60 beam profile.

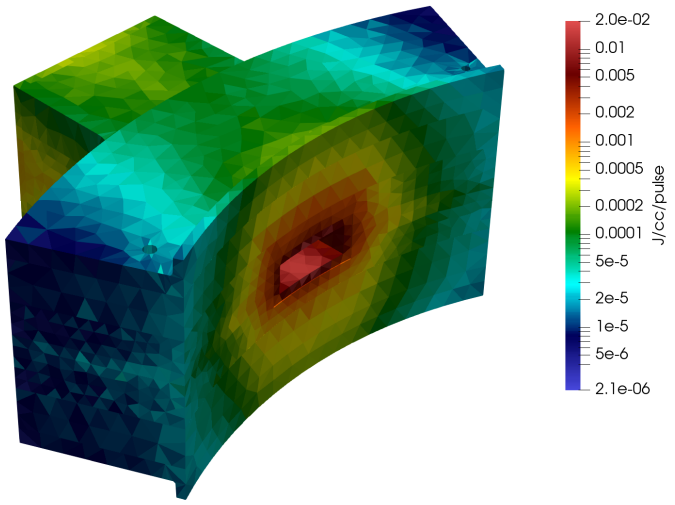

Figure 12. Isometric view of energy deposition in the cooled beltline component for the centered qd60 beam profile.

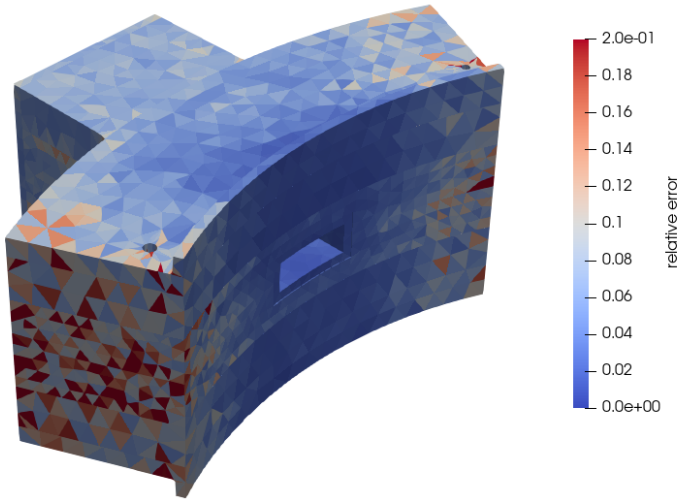

Figure 13. Statistical precision of the energy deposition data in the isometric view in the cooled beltline component for the centered qd60 beam profile.

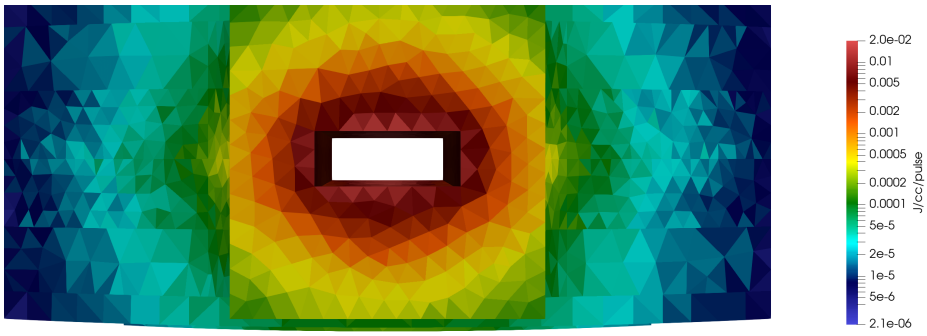

Figure 14. Three-dimensional view in the +X direction (beam going in the page) of energy deposition in the cooled beltline component for the centered qd60 beam profile.

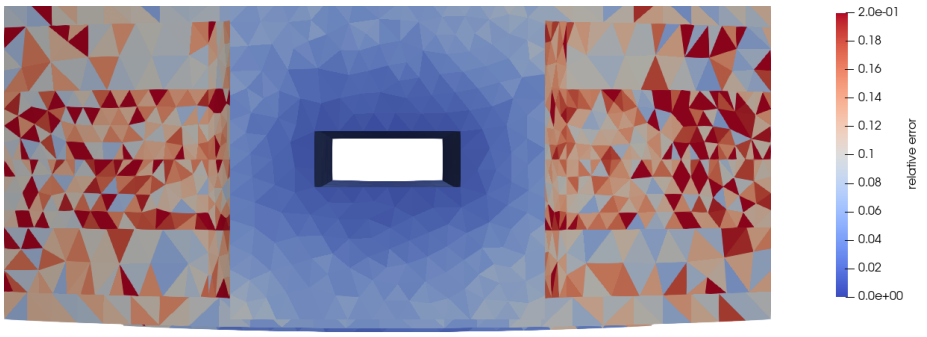

Figure 15. Statistical precision of the energy deposition data in the +X direction view in the cooled beltline component for the centered qd60 beam profile.

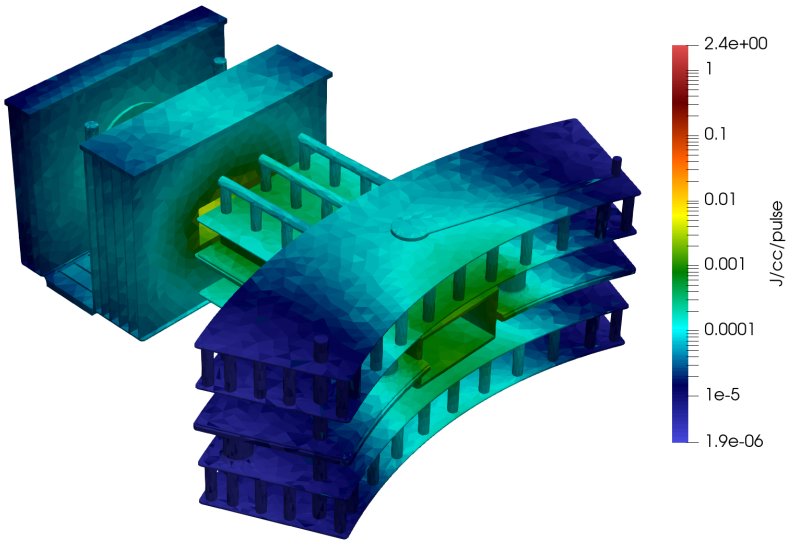

Figure 16. Isometric view of energy deposition in the water for the centered qd60 beam profile.

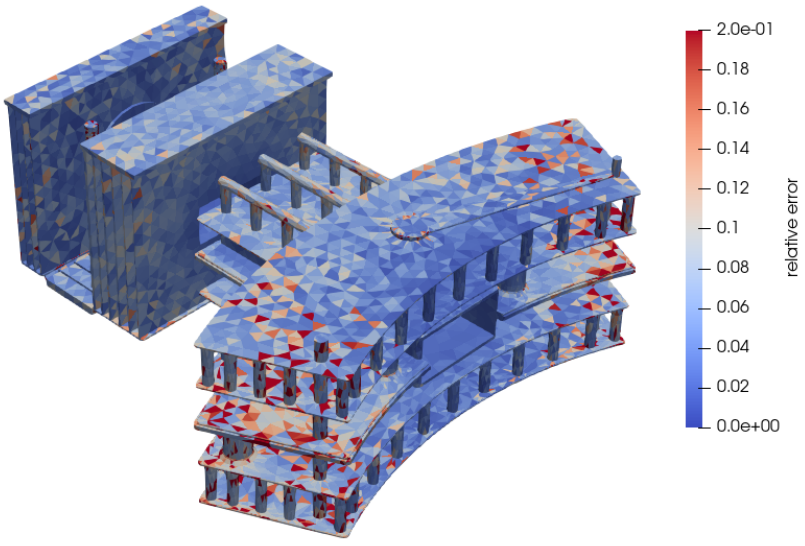

Figure 17. Statistical precision of the energy deposition data in the water in the isometric view for the centered qd60 beam profile.

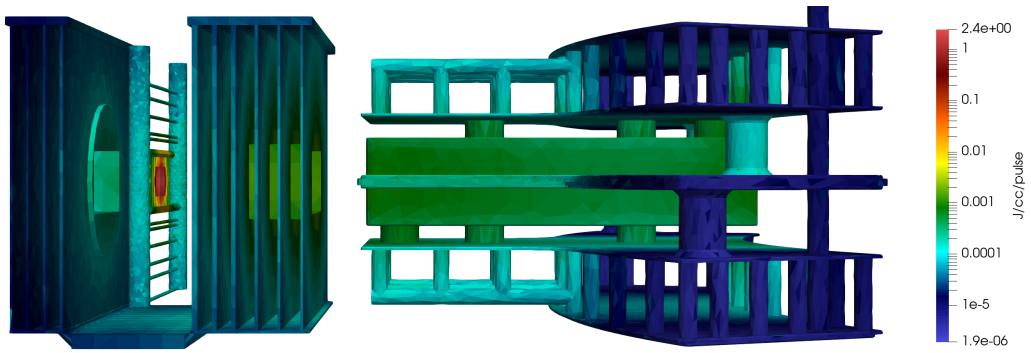

Figure 18. Three-dimensional view in -Z direction of energy deposition in the water for the centered qd60 beam profile.

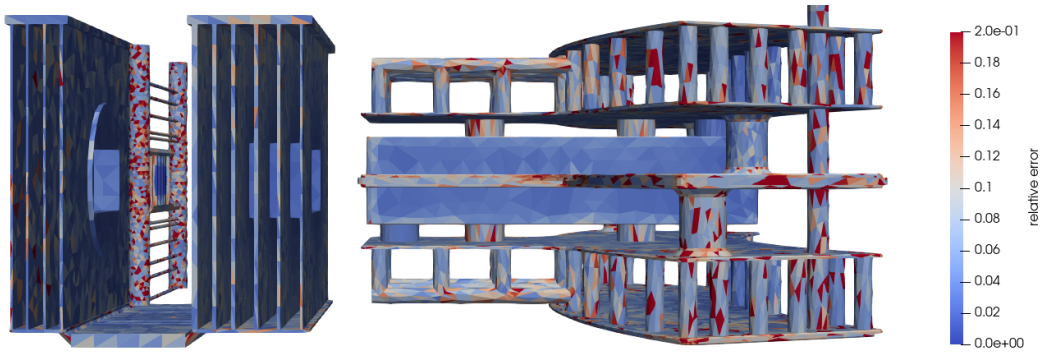

Figure 19. Statistical precision of the energy deposition data in the water in the -Z direction view for the centered qd60 beam profile.